

Ultrasensitive absorption spectroscopy with a high-finesse optical cavity and off-axis alignment

Joshua B. Paul, Larry Lapson, and James G. Anderson

A simple and easy to use method that allows high-finesse optical cavities to be used as absorption cells for spectroscopic purposes is presented. This method introduces a single-mode continuous-wave laser into the cavity by use of an off-axis cavity alignment geometry to eliminate systematically the resonances commonly associated with optical cavities, while preserving the absorption signal amplifying properties of such cavities. This considerably reduces the complexity of the apparatus compared with other high-resolution cavity-based absorption methods. Application of this technique in conjunction with either cavity ringdown spectroscopy or integrated cavity output spectroscopy produced absorption sensitivities of $1.5 \times 10^{-9} \text{ cm}^{-1} \text{ Hz}^{-1/2}$ and $1.8 \times 10^{-10} \text{ cm}^{-1} \text{ Hz}^{-1/2}$, respectively. © 2001 Optical Society of America

OCIS codes: 000.2170, 120.2230, 120.6200, 280.3420, 300.1030, 300.6260.

1. Introduction

For decades, theory has predicted the ability of Fabry–Perot optical cavities to provide absorption path lengths equivalent to multipass cells with tens of thousands of passes.^{1,2} However, any method seeking to take advantage of this property must account for the interferometric cavity resonances that arise because of the periodic boundary condition imposed by the mirror surfaces. In fact, only recently have there been reports that approach predicted levels of sensitivity, and this has been achieved only when a single-frequency laser is locked to a single resonance mode of the cavity.^{3,4} Unfortunately, this places extreme demands on the stability of the apparatus and is therefore complex and expensive to implement.

Numerous other cavity-based approaches have been reported that offer lower sensitivity but are also far less complex.^{5,6} In 1988, for example, pulsed-laser cavity ringdown spectroscopy (CRDS) was introduced, which avoids much of this complexity by use of short-coherence-length lasers (compared with

the cavity length), ensuring that the laser bandwidth spans several longitudinal cavity modes.⁷ Under these conditions, the wavelength-independent average of the cavity transmission spectrum [integrated over the free spectral range (FSR) of the cavity, for example] dictates the observed cavity transmission characteristics. This allows a constant fraction of the incident laser power to be coupled through the cavity for each laser shot while the cavity remains passive, regardless of the laser center wavelength. Unfortunately, although modest gains in sensitivity have been reported over the years, the sensitivity of pulsed-laser methods continues to fall well short of resonant-coupling approaches.

Other cavity-based methods have been introduced recently that, like pulsed CRDS, rely on broadband cavity transmission characteristics, but employ narrow-band cw lasers rather than pulsed lasers. This is achieved by means of monitoring the cavity transmission while averaging the cavity mode structure, either by oscillating the cavity length⁸ or by antimode matching the laser with the cavity such that the laser couples to a large number of transverse cavity modes.⁹ These approaches were designated as integrated cavity output spectroscopy (ICOS) and cavity-enhanced absorption spectroscopy, respectively. Although both approaches demonstrate sensitivities comparable with those obtained with pulsed CRDS, the ability of these methods to utilize compact, high-resolution semiconductor lasers without active frequency-locking schemes is appealing, particularly

J. B. Paul (josh@huarp.harvard.edu), L. Lapson, and J. G. Anderson are with the Department of Chemistry and Chemical Biology, Harvard University, Cambridge, Massachusetts 02138-0000.

Received 2 February 2001; revised manuscript received 21 May 2001.

0003-6935/01/274904-07\$15.00/0

© 2001 Optical Society of America

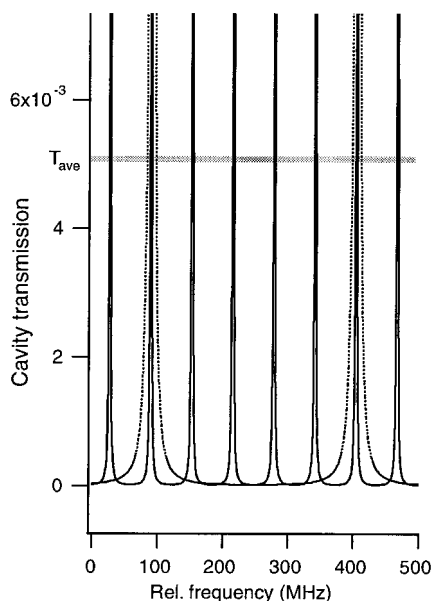


Fig. 1. Predicted cavity-mode structure for an ~ 50 -cm cavity aligned on axis (dotted curve) and off axis in a 10-pass configuration (solid curve). The gray bar indicates the frequency-averaged transmission level.

within the context of producing trace gas sensors that are robust, low-cost, and portable.

The limiting noise source in both ICOS and cavity-enhanced absorption spectroscopy was clearly in the ability to average the cavity frequency response function effectively, which directly translated to noise in the resulting absorption spectrum. In this paper, we address this issue by aligning the laser in an off-axis configuration with respect to the optical cavity, instead of using the conventional on-axis alignment, to create an extremely dense-mode spectrum. The alignment patterns used here are common in multipass absorption cells, but were actually first explored in conjunction with optical cavities.¹⁰ These early studies demonstrated a dramatic decrease in the effective cavity FSR for certain cavity alignment geometries. Here, this property is used to average the cavity transmission spectrum more effectively, resulting in an order-of-magnitude improvement in sensitivity.

To illustrate this, consider Fig. 1, which shows the expected cavity transmission versus frequency (i.e., Airy functions derived from Fabry–Perot theory) for a 50-cm cavity with 99% reflective mirrors aligned on axis (dotted curve) and off axis with a five round-trip reentrant condition (solid curve). Although the poles in the transmission spectrum extend to unity, for clarity, only the lower regions of the curves are shown. Note that the cavity finesse, given by the ratio of mode spacing to mode width, remains constant as required to conserve energy. Similarly, the average transmission (i.e., integrated over one FSR), shown by the solid gray bar in Fig. 1, also remains constant. As the reentrant condition lengthens, the mode spacing continues to collapse. On the other

hand, the mode width will eventually reach a lower limit dictated primarily by mechanical fluctuations in the system and irregularities in the mirror surfaces. At this point, the Fabry–Perot theory breaks down. Consequently, the peak transmission begins to fall, again to conserve energy. The limiting case in this situation is clearly the desired one, in which the cavity resonances are effectively suppressed. In this regime, the cavity transmission is frequency independent and is therefore determined solely by the round-trip cavity loss.

The present approach offers several additional advantages. Simply adding a standard mechanical chopper wheel and a simple two-lens telescope allows us to perform CRDS measurements. This is quite helpful because ICOS provides only relative absorption data unless the intrinsic cavity loss is known, which is easily determined with CRDS. In fact, both measurements can be made simultaneously. In addition, we can use extremely narrow-band lasers ($\Delta\nu < 1$ MHz) without controlling the cavity length. This eliminates the need for expensive components such as acousto-optic modulators, piezoelectric transducers, and lock-in amplifiers. Furthermore, the off-axis design reduces the optical feedback from the cavity to the source laser, which can be problematic for diode lasers. Previously, either Faraday isolators, which are expensive and not available over much of the infrared spectrum, or ring cavities¹¹ have been used for this purpose. Finally, the constraints on the overall system alignment are reduced. Rather than a single possible alignment geometry (i.e., the laser on axis with the cavity), a virtually infinite number of stable paths through the cavity can be used. This allows for simpler alignment routines and lowers the sensitivity of the instrument to vibration and misalignment.

The potential drawbacks to this approach include the significantly lower power transmission through the cavity compared with resonant-coupling methods and the loss of spatial resolution in the probe axis that is due to the off-axis injection. In many cases, however, these are not limiting factors, particularly when moderately high-power lasers or sensitive detectors are available and when the sample of interest is not confined to a small area, such as in many environmental monitoring applications.

2. Theory

Off-axis paths through optical cavities were first investigated in the mid-1960s.^{10,12} These configurations spatially separate the multiple reflections within the cavity until the reentrant condition is fulfilled, referring to the time at which the ray begins to retrace its original path through the cavity. This occurrence condition is dictated by the specific curvature and spacing of the mirrors forming the cavity. Any stable cavity geometry can produce stable off-axis paths through the cavity, with the stability con-

dition (for a spherical two-mirror cavity) defined by the inequality

$$0 < (1 - d/R_1)(1 - d/R_2) < 1, \quad (1)$$

where d is the mirror spacing and R_1 and R_2 are the mirror curvatures. The multiple reflections appear on the mirrors as a series of spots in an elliptical pattern. The per-pass rotation (θ) around the ellipse is again determined purely by the geometry of the cavity and is given by

$$\cos \theta = 1 - d/R, \quad (2)$$

assuming $R = R_1 = R_2$. When $m2\theta = n2\pi$, where m equals the number of optical round-trip passes and n is an integer, the pattern becomes reentrant. For certain conditions, this occurs after only a few passes; however, for others the number of passes can approach infinity. In many respects, the properties of the cavity, including the FSR, become similar to one that is m times longer. For example, a 0.5-m cavity normally has a FSR of 300 MHz; however, one aligned in a 100-pass configuration (50 round trips) has an effective FSR of only 6 MHz. We can further lengthen the reentrant condition to more than 1000 passes by using astigmatic mirrors, which results in a Lissajous spot pattern.¹² For the present application, a specific pattern (or even a known pattern) is not required, as the light is not extracted from the cavity by means of a hole in the mirror. This fact removes much of the complications associated with use of astigmatic mirror cavities for absorption spectroscopy.¹³

Once a condition is achieved in which the effective cavity FSR is significantly narrower than the laser bandwidth, the fringe contrast ratio approaches unity, implying that the amount of energy coupled into the cavity ceases to be a function of laser wavelength.¹⁴ In practice, the more important ratio is between the cavity FSR and the width of the absorption feature of interest because, even if the first condition is not met, the laser frequency can be either dithered or simply rapidly scanned through the cavity modes to reduce the fringe contrast while a sufficient number of data points are retained to define the absorption feature.

With these conditions met, all wavelength and electric field phase information can be neglected, leading to a simplified description of the intracavity optical intensity. To account for the presence of a cw laser directed into the cavity, a source term is added to the standard differential equation used to describe the ringdown event.⁵ The rate equation describing the change in the intracavity power (traveling in each direction) becomes

$$\frac{dI}{dt} = \frac{c}{2L} [I_L C_p T - 2I(1 - R)], \quad (3)$$

where I_L is the incident laser power, C_p is a cavity coupling parameter, R and T are the mirror intensity reflection (not to be confused with radius of curva-

ture) and transmission coefficients, L is the cavity length, and c is the speed of light. The factor of 2 in the loss term accounts for the fact that the light leaves through both mirrors, whereas it enters through only one. C_p has a value between 0 and 1 and generally depends on the spatial-mode quality of the light source and the degree of mode matching between the cavity and the laser. For pulsed lasers, this value is often fairly low (~ 0.1), but it can approach unity for a well-matched TEM₀₀ cw laser. When we assume a stable light source, the solution to Eq. (3) for an initially empty cavity is

$$I = \frac{I_L C_p T}{2(1 - R)} [1 - \exp(-t/\tau)]. \quad (4)$$

When the laser is switched on, a ring-up occurs with the same time constant as the ringdown, given by $\tau = L/[c(1 - R)]$. Steady state is reached when $I = I_L C_p T/[2(1 - R)]$ in each direction, i.e., the amount transmitting through the rear mirror is $\approx I_L C_p T/2$ (assuming $R + T \approx 1$). In other words, at steady state half of the laser power coupling into the cavity leaves through each mirror, as required to conserve energy. In general, this result represents the broadband steady-state transmission of any high-finesse etalon, as it also corresponds to the integral of the Airy function over one FSR.¹⁴ Once sufficient laser power leaves the cavity, the laser can be quickly interrupted to observe the ringdown decay. As the intensity buildup occurs predictably, this can be done with a passive device such as a mechanical chopper.

With an absorbing medium between the mirrors, R is replaced by R' , given by

$$R' = R \exp[-\alpha(\omega)]. \quad (5)$$

where $\alpha(\omega)$ represents the absorbance of the medium over the length of the cavity. Thus we can determine the intracavity absorption by comparing the cavity decay times with and without the absorber present because comparing Eq. (5) with the Beer-Lambert absorption formula for a single pass through the medium $\{I/I_0 = \exp[-\alpha(\omega)]\}$ reveals that $I/I_0 = R'/R$. Equations (4) and (5) also show that absorption information is contained in the steady-state cavity output intensity, which is essentially the basis for ICOS. From Eqs. (4) and (5), it is easy to show that the change in steady-state output that is due to the presence of an absorbing species is given by

$$\frac{\Delta I}{I} = \frac{GA}{1 + GA}, \quad (6)$$

where $A = 1 - \exp[-\alpha(\omega)]$ and $G = R/(1 - R)$. For weak absorption ($GA \ll 1$), the cavity provides a linear absorption signal gain (Fig. 2). Therefore G is referred to as the gain of the cavity. For example, a gain of 10^4 [$1 - R = 100$ parts per million (ppm)] would result in a 1% change in cavity output power for an absorption A of 1 ppm. Physically, G corresponds to the number of optical passes that occur within the cavity decay time ($G \equiv \tau c/L$) and is also

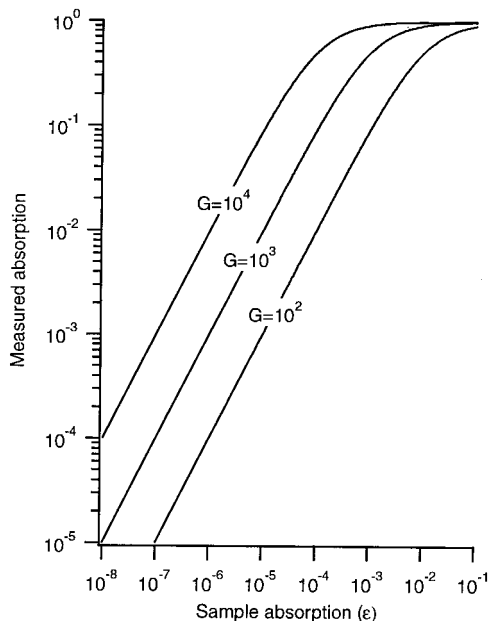


Fig. 2. Effective cavity gain as a function of the gain parameter G and intracavity absorption.

simply related to the cavity finesse ($G \cong F/\pi$). Also clear from Fig. 2 is that, as the absorption becomes comparable to the intrinsic cavity loss, the gain rolls off as the absorption begins to limit the effective number of passes rather than the losses at the mirrors.

The above analysis shows that the cavity provides tremendous signal gains even if the cavity resonances are completely suppressed. In fact, the nonresonant gain is reduced only by a factor of 2 compared with the expected gain when the laser is resonantly coupled to a single cavity mode.³ This factor relates to the relative change between the peak and the integrated area of an individual Lorentzian cavity mode for a given intracavity absorbance. The transmitted power level, on the other hand, is reduced by a factor of $\sim T/2$, or 2×10^4 for $T = 100$ -ppm mirrors. Therefore moderately powerful lasers and sensitive detectors are certainly desirable to achieve high sensitivity with this method. In terms of the ultimately achievable shot-noise limit, however, the difference between the two methods is only $\sqrt{T}/2$ for a given source laser power, or a factor of 140 in the current example. It should also be noted that the cavity time constant places an upper limit on the rate of data collection. In terms of amplitude response, the cavity acts as a single-pole, low-pass filter with a roll-off frequency ($\nu = 1/2\pi\tau$) that ranges from ~ 5 to 50 kHz, depending on the reflectivity of the mirrors.

We chose the specific cavity geometry used here following numerical simulations of a variety of cavity designs using a simple geometric ray transfer matrix formalism.¹⁵ These include near confocal and the commonly used spacing near the limit of stability of slightly less than twice the mirror radius of curvature. Although each of these possibilities could be used to create a dense cavity-mode spectrum, the long

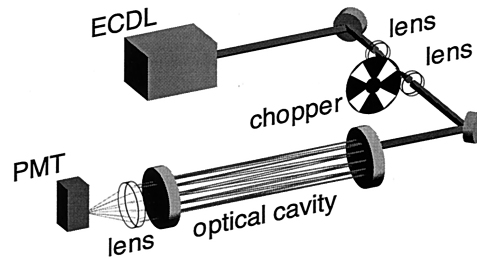


Fig. 3. Schematic diagram of the present experimental apparatus. The optical cavity is aligned off axis to spoil the resonances commonly associated with Fabry-Perot etalons. The entire cavity output is focused onto the photomultiplier tube (PMT) to record the ringdown signal.

focal-length condition was found to be the least sensitive to changes in both alignment and mirror spacing. In addition, the pattern of light emerging from such a cavity could be focused to the smallest area. Although this is not a big concern when large-area photomultiplier tubes (PMTs) are available, it becomes important for infrared applications in which small detector element sizes are preferred to reduce noise. Furthermore, if the detector does not capture all the light leaving the cavity, undesirable fluctuations in the signal could occur as the detector acts as a spatial filter. Finally, when we ensure that the focused pattern is smaller than the detector area, it guards against small drifts in the system alignment from causing large changes in the observed signal. According to the simulations, the present cavity configuration allows a 0.75-in.- (1.9-cm-) diameter pattern emerging from the cavity to be focused to a diameter of <0.5 mm with a single 1 in.- (2.54-cm-) diameter $F/1$ lens.

3. Experiment

A schematic experimental diagram is shown in Fig. 3. The optical cavity consisted of two identical 6-m radius-of-curvature, 1-in.- (2.54-cm-) diameter mirrors (Research Electro-Optics, Inc.) spaced 67 cm apart. The mirrors were coated for maximum reflectivity at 585 nm, but managed a respectable per mirror intensity loss of 235–300 ppm ($G \approx 4000$) at 630 nm, depending on their state of cleanliness. The ringdown cavity and a 2–3-mW external-cavity diode laser (ECDL) (New Focus Model 6304) were mode matched by use of a two-lens telescope. A mechanical chopper placed at the focal point between the telescope lenses interrupted the beam with a 50% duty cycle at a 3-kHz repetition rate for CRDS measurements. This arrangement provided a shut-off time of the laser into the cavity of <0.5 μ s. The light exiting the cavity was focused by a lens, filtered by a narrow-bandpass interference filter, and detected by a PMT. A variable bandwidth, variable gain amplifier (Stanford Research Systems SR560) was employed following the PMT. For CRDS measurements, the amplifier bandwidth was maintained at its widest setting of 1 MHz, and we scanned the ECDL by stepping the voltage to the piezoelectric

transducer controlling the laser end-mirror position by computer, which provided 2 cm^{-1} of continuous tunability. For ICOS, the amplifier bandwidth was reduced to 3 kHz, and a 10-Hz voltage ramp from a function generator was supplied to the laser piezoelectric transducer, providing an effective spectral resolution of $\sim 200\text{ MHz}$. The signal was then sent to a digital storage oscilloscope (Tektronix TDS540), which was controlled by a general-purpose interface bus from a standard PC. LabVIEW software was used to control the experiment and to process the data.

The off-axis cavity alignment proved to be straightforward and reproducible and could usually be accomplished in under 5 min when we used the following procedure. We first align the laser and the cavity coaxially by centering the laser with respect to both mirrors and adjusting the mirrors such that the returning beams overlapped the incoming beam. At this point, any light leaving the cavity through the rear mirror would reveal a uniform spot with a minimum of non-TEM₀₀ structure, along with large power fluctuations in random intervals corresponding to mode coincidences between the laser and the unstabilized cavity. The final turning mirror in front of the cavity is then moved orthogonally $\sim 1\text{ cm}$ with respect to the cavity axis. Following this, the light path through the cavity would trace out a horizontal line on each mirror. With a small adjustment of the same turning mirror in the vertical direction, the light path traces out a circle on each cavity mirror. Finally, we induce a slight astigmatism in the mirror curvature by modestly tightening the set screw, which secures the mirror in the kinematic mount.

4. Results and Discussion

A. Off-Axis Injection

Figure 4 shows images observed by a video camera through the rear cavity mirror. The top pattern in Fig. 4 closely matches that expected from calculations, although individual spots are not observed because the resulting image is actually the sum of thousands of slightly displaced spots. When we astigmatize the mirrors, it produces the expected Lissajous pattern (Fig. 4, bottom). This lengthens the reentrant condition compared with the spherical mirror case, decreasing the cavity-mode spacing. However, at constant wavelength, large power fluctuations through the cavity were observed even with astigmatic mirrors. These fluctuations, which pay tribute to the extremely long coherence length of the ECDL ($>2\text{ km}$), occurred on millisecond time scales, in contrast with the microsecond events observed for on-axis alignment. In fact, the Lissajous pattern could be observed to breathe with the room air currents and would at times disappear all together, leaving just a patch of light on the mirror. Despite these fluctuations, at no time did the cavity output drop to zero, such that at any time the laser could be interrupted to observe a ringdown event.

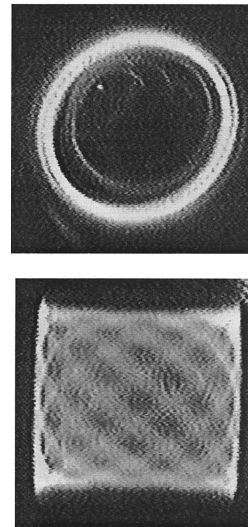


Fig. 4. Images obtained by a video camera looking through the rear mirror of the cavity showing the off-axis cavity alignment patterns. Top, spherical mirrors; bottom, astigmatic mirrors.

Presumably, larger-diameter mirrors could be used to increase the power stability in the cavity. This would allow the multiple beams in the cavity to be spread over a larger area, thus decreasing their interaction.

Scanning the laser at a rate exceeding $2\text{ cm}^{-1}\text{ s}$ stabilized the cavity power output considerably, which implies an effective cavity FSR in the neighborhood of 500 kHz, or a reentrant condition that exceeds 400 passes. This estimate assumes that, when the laser is scanned through one effective FSR within the ringdown time, this is sufficient to suppress resonant energy buildup in the cavity and is consistent with previous results for astigmatic mirror cavities.^{12,13} The above tuning rate, along with the 16-kHz cavity bandwidth, corresponds to an effective frequency resolution $\sim 25\text{ MHz}$.

B. Cavity Ringdown Spectroscopy

With the chopper wheel spinning, buildup ringdown events occur at a high repetition rate, in this case, 3 kHz (Fig. 5). An average of 20 individual decay waveforms is shown in Fig. 6, which exhibits a smooth exponential function. Incidentally, no difference in cavity decay time was observed for on-versus off-axis alignment. When the laser frequency is scanned, it produces an absorption spectrum such as the one shown in the top panel of Fig. 7, in which the $P(8)$ line of the oxygen γ band was detected directly in the laboratory atmosphere with a 67-cm open-path cavity. Each point in this scan represents an average of 50 individual decay waveforms. Although this spectrum corresponds to 7 s of data collection (21,000 shots at 3 kHz), the actual scan took considerably longer because of gross inefficiencies in the data collection system, which are presently being addressed. The rms fluctuations in these data are 0.8 ppm, which correspond to an uncertainty in the time-constant determination of 3×10^{-3} and a

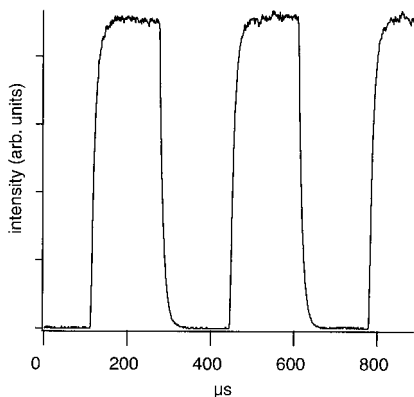


Fig. 5. Buildup ringdown cycle measured with the chopper activated.

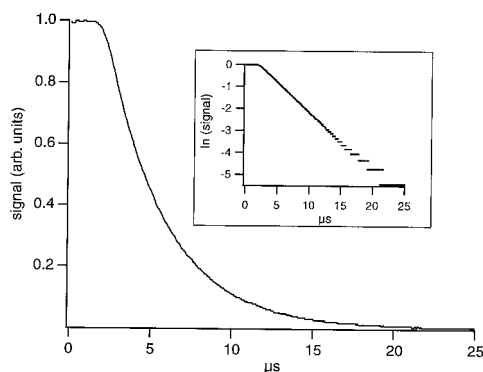


Fig. 6. Measured ringdown decay signal by use of the present off-axis cavity ringdown method. Inset: the natural logarithm of the signal is linear, indicating a single exponential decay.

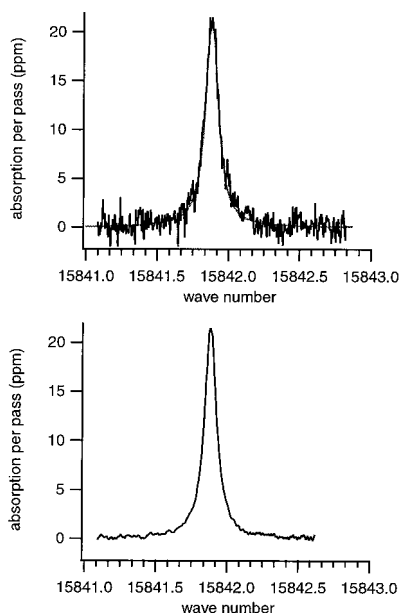


Fig. 7. Top, the $P(8)$ line of the molecular oxygen γ band as measured with CRDS. Also shown is the HITRAN prediction based on an atmospheric O_2 abundance of 21%. Bottom, the same line measured immediately afterward with ICOS.

rms fractional absorption sensitivity of $1.5 \times 10^{-9} \text{ cm}^{-1} \text{ Hz}^{-1/2}$. Although this sensitivity is consistent with the limitations of an 8-bit digitizer, unfortunately, one with a higher bit depth was not available. As expected, this system was found to be largely insensitive to vibrations and slight changes in alignment.

It should be noted that the diode laser used in these experiments was not properly functioning, as a degraded antireflection coating on the diode endface conspired with the operation of the laser near the edge of its tuning range to produce periods lasing between the diode endfaces in addition to the desired laser emission from the external-cavity mode. The undesired emission consisting of ~ 20 laser modes was redshifted from the primary laser line by $\sim 10 \text{ nm}$ and accounted for up to 30% of the total output power. To improve the quality of the data, the temperature of the laser was adjusted such that the excess laser emission was at a minimum near the absorption line. This manifested itself as a low-frequency oscillation in the spectrum with a period equal to the FSR of the laser diode ($\sim 2 \text{ cm}^{-1}$), which was removed from the data in Fig. 7.

These results compare favorably with those commonly obtained with pulsed-laser ringdown, which is attributable to the high repetition rate of the present configuration and the stability offered by the solid-state cw laser source. The notable exception here is the research of van Zee and co-workers,¹⁶ which demonstrated per-shot time-constant uncertainties of 3×10^{-4} , but required a fairly elaborate setup consisting of a single-mode pulsed laser and a short, temperature-stabilized cavity that tracked in frequency with the laser. The present results also compare favorably with the cw laser-based method of Romanini *et al.*¹⁷ after we accounted for the difference in mirror reflectivity between their research and ours. However, these results fall well short of those obtained by a CRDS method that maintains a continuous frequency lock between the laser and the cavity, which provided a sensitivity of $9 \times 10^{-12} \text{ cm}^{-1} \text{ Hz}^{-1/2}$.⁴

We believe that the present results could be improved in several ways. The obvious way would be to obtain higher-reflectivity mirrors, as mirrors with over an order-of-magnitude higher reflectivity are available. Of course this would reduce the detected power by at least the same amount, so it is likely that a more powerful laser would be necessary as well. This, however, does not present a problem because vastly more powerful tunable diode-laser systems than the one used presently are commercially available. In addition, use of a higher bit-depth digitizer, an increase in the duty cycle of the experiment, use of more stable mechanical components, and use of a closed-cell gas-sampling system are all likely to improve the results.

C. Integrated Cavity Output Spectroscopy

To record an ICOS spectrum, the laser was scanned over a 2-cm^{-1} frequency interval at a repetition rate

of 10 Hz with the chopper wheel deactivated. This scan rate corresponds to an effective frequency resolution of 200 MHz, based on the 3-kHz acquisition bandwidth. The noise level during a single sweep corresponded to a fractional absorption of ~ 1 ppm, such that the 21.5-ppm absorption feature could be easily observed in real time with a 0.1-s update interval. When we averaged for 10 s (100 sweeps), we produced the data shown in Fig. 7 (bottom panel). The rms signal-to-noise ratio demonstrated here is >200 , which corresponds to a per-pass fractional absorption sensitivity of 1×10^{-7} . Incidentally, these measurements also suffered from the problems with the laser described above, which caused periods of additional noise in the measurement. We observed absorption-equivalent noise levels as small as 6.5×10^{-8} or $1.8 \times 10^{-10} \text{ cm}^{-1} \text{ Hz}^{-1/2}$ based on the 3-kHz detection bandwidth and the number of averaged cycles between these periods. This result is within a factor of 50 of the shot-noise limit based on the estimated optical power received by the detector and represents an order-of-magnitude gain in sensitivity over previous ICOS approaches.^{8,9} Again, the present results fall well below those of a recent cavity-locked method³; however, it should be remembered that the present approach is much simpler to implement and requires far fewer expensive components.

Although ICOS presently shows an order-of-magnitude greater sensitivity than CRDS, much of this difference can be accounted for when we simply consider the disparity between the acquisition duty cycle of the two methods. With CRDS, approximately 15 ms of data was collected every 333 ms (3-kHz repetition rate), yielding an effective duty cycle of 4.5%. Therefore, when compared with the unity duty cycle of ICOS, we expect the CRDS sensitivity to be reduced by a factor of 5. The remaining factor of 2 can most likely be accounted for by the inadequate bit depth of the digitizer mentioned above, combined with the use of a simple unweighted fitting routine for the exponential decay fits.

Not surprisingly, many of the suggested improvements for the CRDS measurements also apply for ICOS. In particular, higher-reflectivity mirrors would increase the absorption signal, and more laser power would increase the signal on the detector and allow intrinsically low-noise detectors such as photodiodes to be employed. In addition, the filtering spatial mode of the laser could potentially reduce noise by further reducing the residual cavity resonances. Larger-diameter mirrors could also be used to improve this area as well by allowing longer reentrant conditions to be obtained.

5. Conclusions

We have demonstrated a remarkably simple and effective method that allows cw diode-laser sources to be used in conjunction with high-finesse optical cavities to perform ultrasensitive absorption spectroscopy.

This method uses off-axis alignment to render unnecessary many of the expensive components used previously in these endeavors. We have recently extended these results into the mid-infrared region using quantum-cascade lasers, which will be described in a future publication.

J. B. Paul thanks the Henry and Camille Dreyfus Foundation Postdoctoral Research Program for support.

References

1. D. A. Jackson, "The spherical Fabry-Perot interferometer as an instrument of high resolving power for use with external or with internal atomic beams," *Proc. R. Soc. London Ser. A* **263**, 289–308 (1961).
2. G. Hernandez, "Fabry-Perot with an absorbing etalon cavity," *Appl. Opt.* **24**, 3062–3067 (1985).
3. J. Ye, L.-S. Ma, and J. L. Hall, "Ultrasensitive detections in atomic and molecular physics: demonstration in molecular overtone spectroscopy," *J. Opt. Soc. Am. B* **15**, 6–15 (1998).
4. T. G. Spence, C. C. Harb, B. A. Paldus, R. N. Zare, B. Wilke, and R. L. Byer, "A laser-locked cavity ring-down spectrometer employing an analog detection scheme," *Rev. Sci. Instrum.* **71** (2), 347–353 (2000).
5. J. J. Scherer, J. B. Paul, A. O'Keefe, and R. J. Saykally, "Cavity ringdown laser absorption spectroscopy—history, development, and application to pulsed molecular beams," *Chem. Rev.* **97** (1), 25–51 (1997).
6. G. Berden, R. Peeters, and G. Meijer, "Cavity ring-down spectroscopy: experimental schemes and applications," *Int. Rev. Phys. Chem.* **19** (4), 565–607 (2000).
7. A. O'Keefe and D. A. G. Deacon, "Cavity ring-down optical spectrometer for absorption measurements using pulsed laser sources," *Rev. Sci. Instrum.* **59**, 2544–2551 (1988).
8. A. O'Keefe, J. J. Scherer, and J. B. Paul, "CW integrated cavity output spectroscopy," *Chem. Phys. Lett.* **307** (5–6), 343–349 (1999).
9. R. Engeln, G. Berden, R. Peeters, and G. Meijer, "Cavity enhanced absorption and cavity enhanced magnetic rotation spectroscopy," *Rev. Sci. Instrum.* **69**, 3763–3769 (1998).
10. D. R. Herriott, H. Kogelnik, and R. Kompfner, "Off-axis paths in spherical mirror interferometers," *Appl. Opt.* **3**, 523–526 (1964).
11. B. A. Paldus, C. C. Harb, T. G. Spence, B. Wilke, J. Xie, J. S. Harris, and R. N. Zare, "Cavity-locked ring-down spectroscopy," *J. Appl. Phys.* **83**, 3991–3997 (1998).
12. D. R. Herriott and H. J. Schulte, "Folded optical delay lines," *Appl. Opt.* **4**, 883–889 (1965).
13. J. B. McManus, P. L. Kebarian, and M. S. Zahniser, "Astigmatic mirror multipass absorption cells for long-path-length spectroscopy," *Appl. Opt.* **34**, 3336–3348 (1995).
14. K. K. Lehmann and D. Romanini, "The superposition principle and cavity ring-down spectroscopy," *J. Chem. Phys.* **105**, 10263–10277 (1996).
15. J. G. Xin, A. Duncan, and D. R. Hall, "Analysis of hyperboloidal ray envelopes in Herriot cells and their use in laser resonators," *Appl. Opt.* **28**, 4576–4584 (1989).
16. R. D. van Zee, J. T. Hodges, and J. P. Looney, "Pulsed, single-mode cavity ringdown spectroscopy," *Appl. Opt.* **38**, 3951–3960 (1999).
17. D. Romanini, A. A. Kachanov, and F. Stoeckel, "Diode laser cavity ring down spectroscopy," *Chem. Phys. Lett.* **270** (5–6), 538–545 (1997).